JACS
JOURNAL OF THE AMERICAN CHEMICAL SOCIETY

Communication

pubs.acs.org/JACS

Monitoring the Solid-State Electrochemistry of Cu(2,7-AQDC) (AQDC = Anthraquinone Dicarboxylate) in a Lithium Battery: Coexistence of Metal and Ligand Redox Activities in a Metal–Organic Framework

Zhongyue Zhang,[†] Hirofumi Yoshikawa,*[,†] and Kunio Awaga*[,†,‡]

[†]Department of Chemistry and Research Center for Materials Science (RCMS), Nagoya University, Furo-cho, Chikusa-ku, Nagoya 464-8602, Japan

[‡]Core Research for Evolutional Science and Technology (CREST), Furo-cho, Chikusa-ku, Nagoya 464-8602, Japan

Supporting Information

ABSTRACT: By adopting a facile synthetic strategy, we obtained a microporous redox-active metal–organic framework (MOF), namely, Cu(2,7-AQDC) (2,7-H_2AQDC = 2,7-anthraquinonedicarboxylic acid) (**1**), and utilized it as a cathode active material in lithium batteries. With a voltage window of 4.0–1.7 V, both metal clusters and anthraquinone groups in the ligands exhibited reversible redox activity. The valence change of copper cations was clearly evidenced by *in situ* XANES analysis. By controlling the voltage window of operation, extremely high recyclability of batteries was achieved, suggesting the framework was robust. This MOF is the first example of a porous material showing independent redox activity on both metal cluster nodes and ligand sites.

Electrical energy storage materials are considered preeminent alternatives to conventional fossil fuels due to their low cost, renewability and low environmental impact.[1,2] Over the past decade, the evolution of materials has led to numerous innovations in the field. In the recent past, the Li-ion battery (LIB) is the pioneer technology as it provides both high energy density and large output current.[3] The core cathode active materials conventionally used in the LIBs are layered metal oxides or metal salts, such as $LiCoO_2$[4] or $LiFePO_4$.[5] The incomplete delithiation of their structure[6] and the formation of insulating metal oxide layers at their interface[7] have led to batteries with practical capacities much lower than their theoretical values, as well as degradation through large cycle numbers. As a substitute for metal oxides, organic-based materials have also been widely investigated and employed as cathode active materials. These materials are generally polymers with reversible redox active functional groups.[8] With designable functional groups and flexible structures, these polymers lead to a tunable discharge voltage and ease of thin film fabrication and deposition on the electrodes, which permits an ultrafast charging speed.[9] The drawbacks of organic-based materials are their self-discharge and low theoretical capacities, owing to their dissolution in electrolytes and large molecular weight per electron uptake.[10] To overcome these issues, recent studies by our group focused on the application of molecular clusters, such as "Mn_{12} acetate"[11] and Keggin-type polyoxometalates[12] as novel cathode active materials due to their large electron uptake numbers. The preliminary results inspired us to develop advanced materials by combining the advantages of organic materials and molecular clusters. The practical strategy was to link the metal clusters with redox active organic bridging ligands to form porous coordination polymers (PCPs), which are also well-known as metal–organic frameworks (MOFs).

MOFs have attracted extensive attention for their porosity. As an imitation of zeolites, these materials have been shown to have potential applications in various fields, including gas storage[13] and selection,[14] molecule recognition[15] and enantioselective catalysis.[16] From the perspective of electronic application, although the electrical conductivity and redox activity of MOFs have been investigated,[17] the mechanism of their solid state electrochemical behavior and electron storage properties have rarely been discussed. Given their porosity and crystallinity that leads to large Li-ion accommodation numbers and structural stability respectively, MOFs have great potential as elegant materials of electron storage. To date, however, there have been only a few examinations of these materials, namely, investigation by Férey and Tarascon of Fe-MIL-53 and Fe-MIL-68,[18] in which the redox active sites are Fe(III) centers. In the case of these MOFs, the Li-ion intercalation number is only ~60% of the theoretical value, and the theoretical capacities are lower than 110 $mAh{\cdot}g^{-1}$. Their lack of permanent porosity restricts the Li-ion insertion numbers of these MOFs, which in turn prevents the complete reduction of the Fe(III) centers. The low theoretical capacity also arises from the existence of a redox-innocent ligand(1,4-benzene dicarboxylic acid, BDC). To overcome upper issues, we adopted a facile design strategy to increase the theoretical capacity by introducing redox-active functional groups on the organic ligands. Outstanding gravimetric capacity may be achieved since electron-accepting sites exist on both the metal clusters and ligands of MOF.

Herein we selected 2,7-anthraquinonedicarboxylic acid (2,7-H_2AQDC) as a bridging ligand. Anthraquinone (AQ) exhibits two reversible redox steps with one electron uptake for each. Therefore, as previously reported, both AQ and its sulfide polymers (PAQS) have been employed as cathode active materials in lithium batteries.[19] The solvothermal reaction between 2,7-H_2AQDC and $Cu(ClO_4)_2{\cdot}6H_2O$ in *N*,*N*-dimethylformamide (DMF) led to the formation of a two-

Received: August 9, 2014
Published: November 3, 2014

   dx.doi.org/10.1021/ja508197w | *J. Am. Chem. Soc.* 2014, 136, 16112–16115

dimensional (2-D) metal organic framework with a formula of $\{Cu(2,7\text{-AQDC})(DMF)\}_\infty \cdot x$DMF (**1**·DMF) (See the details in Supporting Information). The framework adopted a Kagome lattice architecture. A single triangular unit of Kagome lattice was composed by the $Cu_2(Ac)_4$ paddlewheel cluster secondary building units (SBUs) as nodes and anthraquinone groups as bridges (Figure 1a). The axial positions of SBUs were occupied

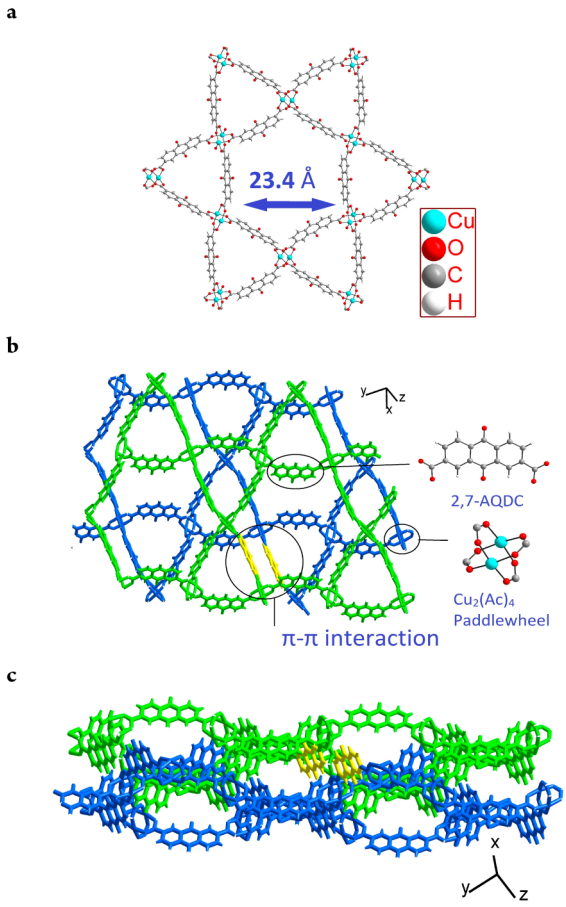

Figure 1. (a) Thermal ellipsoid plot of a single layer of the framework. (b) Top view of Kagome lattice type structure of **1** and a indication figure of glided adjacent layers. The metal cluster junctions were $Cu_2(Ac)_4$ paddlewheels. (c) Side view of two adjacent layers. In all the figures, the axial DMF molecules were omitted for clarity.

by DMF molecules. Hexagonal pores were formed inside the 2-D layers by surrounding AQ groups and possessed a diameter of 23.4 Å, implying that the redox active groups were exposed to the internal surface area. The adjacent layers were glided from perfect eclipse position(Figure 1b). Due to the geometry of the paddlewheel SBUs, the relative position of anthraquinone groups fluctuated periodically around the plane of $Cu_2(Ac)_4$ clusters in the layer, which led to a zigzag structure of 2-D sheets and permitted a weak $\pi-\pi$ interaction between the adjacent layers with a contact distance of 3.43 Å (Figure 1c). Upon the removal of axial DMF molecules that were coordinated with $Cu_2(Ac)_4$ paddlewheel clusters, PLATON/SQUEEZE analysis of the X-ray diffraction data suggested that ~57% of the cell volume was accessible for solvent molecules, implying the porosity of **1**. Although the adjacent layers were not perfectly eclipsed, channels formed by the connection of hexagonal pores appeared in the space-filling diagram (Figure S2). The weak interactions between the layers indicated the structural flexibility of **1**, which could also contribute to a larger practical surface area for the gas adsorption and Li-ion intercalation processes.

Thermal gravimetric analysis was performed on an as-prepared sample of **1**·DMF (Figure S3). Guest DMF molecules were stepwisely expelled from the framework of **1** between 30 and 130 °C, followed by a complete loss of axial DMF at ~175 °C as shown by elemental analysis. The total amount of DMF molecules accounted for ~28% of the weight of as-prepared MOF. After the activation of the as-prepared sample, N_2 adsorption measurement was performed at 77 K, and the Brunauer–Emmett–Teller (BET) fitness suggested a surface area of 631 m^2/g (Figure S4a). Nonlocal density functional theory (NLDFT) analysis of adsorption data provided a pore size distribution of activated **1** that exhibited a single peak at 1.06 nm (Figure S4b). This pore radius agreed well with the hexagonal pore diameter (23.4 Å, radius = 11.7 Å) determined by X-ray diffraction, and illustrated the microporosity behavior of **1**.

CR2032-type coin cell batteries were assembled to characterize the solid state electrochemical behaviors of **1**·DMF. To rule out the kinetic effect and investigate the intrinsic behavior, pellets that contained 10% weight of MOF, 70% carbon black as a conductive additive and 20% PVDF (polyvinylidene fluoride) as a binder were used as cathodes, while the anodes were lithium discs, and a 1:1 v/v EC/DEC (ethylene carbonate/diethyl carbonate) solution of $LiPF_6$ (1 M) was used as electrolyte. In the optimization of the measurement conditions, the voltage window and scan current were selected as 4.0–1.7 V and 1 mA, respectively. Two plateaus were clearly observed in the charge–discharge profile within the voltage ranges of 3.4–2.4 and 2.4–1.7 V, respectively, while the output gravimetric capacity ratio of the two steps was nearly 1:2 (Figure 2a). This phenomenon indicated that two distinct processes with a 1:2 electron uptake ratio occurred during the reduction process. In cyclic performance test of the battery, an

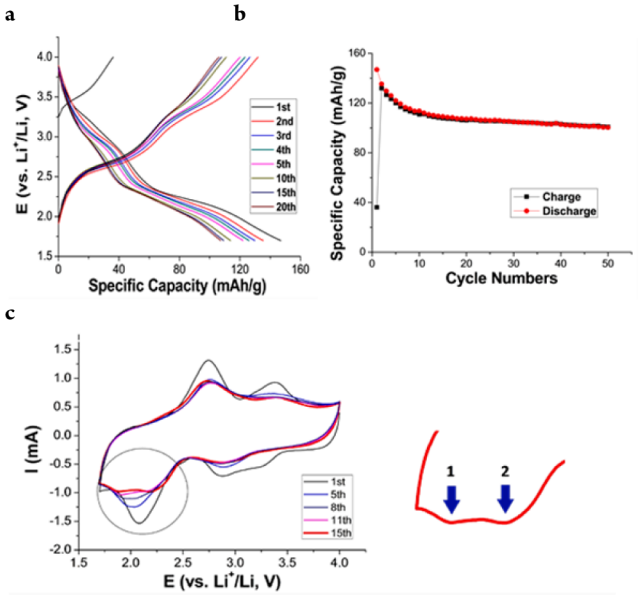

Figure 2. (a) Charge–discharge profile of 10 wt % MOF battery. (b) Cyclic performance of battery in 50 cycles. (c) Cyclic voltammetry plot of battery. Arrows 1 and 2 marked the split of the second reduction peak of the 15th cycle.

dx.doi.org/10.1021/ja508197w | J. Am. Chem. Soc. 2014, 136, 16112–16115

initial specific capacity of 147 mAh/g was achieved, and this capacity rapidly decreased and stabilized to ∼105 mAh/g within 50 cycles (Figure 2b). To further clarify the electrochemical process of MOF reduction, cyclic voltammetry (CV) measurement was also performed on a battery with the same voltage window and a scan rate of 1.0 mV/s. Two isolated reversible peaks with an area ratio of 1:2 appeared at $E_{1/2}$ = 3.1 and 2.4 V, which corresponded to two plateaus in the charge−discharge curve (Figure 2c). During the cycling, the area of both peaks decreased, which also agreed well with the capacity loss in cyclic performance. Interestingly, after 10 cycles, the second reduction peak at ∼2.1 V split into two continuous peaks, which was similar to the preliminary report[19b] and could be identified as a two electron reduction of quinone groups. Therefore, a total uptake of 3 electrons could be achieved based on the formula of {Cu(2,7-AQDC)(DMF)}·x(DMF), which led to a theoretical capacity of ∼162 mAh/g. This theoretical value was close to the initial capacity in the cyclic performance (Figure 2b).

As the reversible peak at $E_{1/2}$ = 2.4 V was assigned to the two electron uptake step of anthraquinone groups, the other peak at $E_{1/2}$ = 3.1 V was naturally assumed to be the redox process between Cu(II) and Cu(I). This hypothesis could be examined by tracking the valence change of copper using *in situ* Cu K-edge X-ray absorption near edge structure (XANES) analysis. A battery reaction cell in our previous study[12b] was adopted for the *in situ* measurement. Interestingly, two steps of absorption edge energy shift were observed within the ranges of 3.48−2.94 and 2.85−2.55 V, respectively (Figure 3). At 3.48 V, the

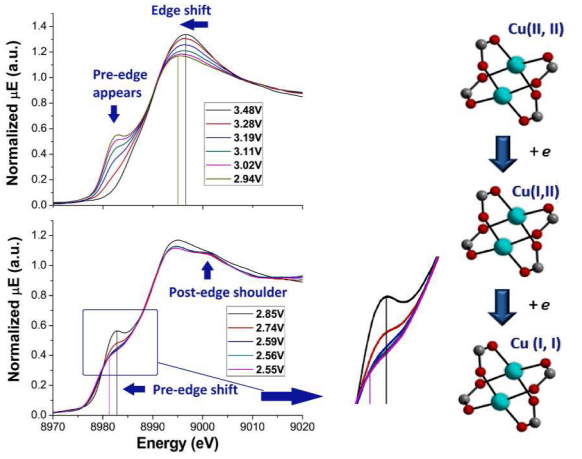

Figure 3. Two steps of edge shift were observed in XANES measurement, which indicated the stepwise reduction of $Cu^{II,II}_2(Ac)_4$ clusters.

spectrum was completely identical to that of the standard sample of as-prepared **1** (Figure S5), while an edge peak shift to the lower energy and the appearance of a pre-edge peak were observed when the voltage decreased to 2.94 V. The pre-edge peak was then shifted to lower energy and another postedge shoulder appeared when the cell voltage decreased to 2.55 V. The spectrum obtained at 2.55 V was similar to the spectrum of the Cu_2O standard, and no more spectrum change could be observed with a further decrease of voltage (Figure S5). The output capacities of these two steps were both ∼28 mAh/g (Figure S6), suggesting an equal electron uptake number of each step. This phenomenon could be assigned to the stepwise electron uptake process of $Cu_2(Ac)_4$ paddlewheel subunits. $Cu_2(Ac)_4$ paddlewheels took one electron in the first step and formed an intermediate state with an average copper valence of 1.5. The increase in copper electron density repulsed acetate groups and promoted the 1s → 4p transition of copper cations, which induced the pre-edge peak. With further reduction, the copper ions were completely reduced to Cu(I), which led to a secondary shift of the K-edge and pre-edge to lower energy. This is the first direct observation of copper acetate reduction in the MOF structures, and also the first example of an MOF that allows both metal clusters and ligands to independently exhibit redox activity.

Although the initial capacity was close to the theoretical value, the battery suffered from a capacity loss of ∼40 mAh/g during a large number of cycles. To investigate the mechanism of the capacity loss, an *ex situ* powder X-ray diffraction study was performed on the cathodes. To obtain reliable diffraction patterns, the weight ratio of MOF in the cathode was increased to 30%. The diffraction peaks were broadened and lost their intensity with the addition of carbon black and PVDF, while the crystallinity of MOF could still be confirmed with the appearance of a (011) peak, and the diffraction pattern was not changed after a discharge, charge and second discharge process (Figure S7). This result suggested that Li-ion intercalation has an insignificant effect on the framework. On the other hand, by narrowing the voltage range to 4.0−2.0 V, an outstanding robustness was achieved for the batteries, and no capacity loss was observed within 50 cycles. A similar high reversibility was also observed in the CV plot: only a minor decrease of peak area was observed for both the oxidation and reduction peaks (Figure S8). Therefore, the MOF framework exhibited great endurance upon the uptake of Li-ions, and thus, the capacity loss may very likely have been due to the insufficient extraction of Li-ions during charge process. Large charge transfer resistance may hinder the movement of Li-ions and prevent some of them from being extracted. The inhomogeneity of crystal size and distribution in the cathodes may limit the exposure of the MOF internal surface to the electrolyte, leading to a partial redox activity of functional groups (Figures S9−S10).

Conclusively, using a straightforward strategy, we clearly obtained the first microporous MOF material with independent redox active sites on both metal and ligands, and we introduced it as a novel cathode active material for lithium batteries. During the discharge process, both $Cu_2(Ac)_4$ paddlewheels and anthraquinone groups were involved in the reduction, as revealed by *in situ* XANES analysis and cyclic voltammetry. Although the theoretical capacity of **1**·DMF was 162 mAh/g, which was comparable to the practical value of major commercial materials (i.e., $LiCoO_2$, 148 mAh/g), the practical capacity was strongly restricted by the limited exposed surface area and low charge transfer rate of MOF materials. These findings suggest that MOF materials with good potential for use in industrial batteries could be induced by fine fabrication techniques, such as the introduction of thin films and nanocrystals. By involving other 3d transition metals, such as Mn, Fe, and Co, new MOFs with larger surface areas and higher reduction voltages might be achieved, which could vastly improve the performance of the MOF-based batteries.

■ ASSOCIATED CONTENT

Supporting Information

The pertinent crystallographical data, the details of physical measurements and the supplementary figures of physical

dx.doi.org/10.1021/ja508197w | J. Am. Chem. Soc. 2014, 136, 16112−16115

measurements. This material is available free of charge via the Internet at http://pubs.acs.org.

AUTHOR INFORMATION

Corresponding Authors

yoshikawah@chem.nagoya-u.ac.jp
awaga@mbox.chem.nagoya-u.ac.jp

Notes

The authors declare no competing financial interest.

ACKNOWLEDGMENTS

We acknowledge the financial support of a Grant-in-Aid for Scientific Research from the Ministry of Education, Culture, Sports, Science, and Technology (MEXT). This work is also supported by the JSPS Core-to-Core Program, A. Advanced Research Networks.

REFERENCES

(1) Armand, M.; Tarascon, J. M. *Nature* **2008**, *451*, 652.
(2) Dunn, B.; Kamath, H.; Tarascon, J. M. *Science* **2011**, *334*, 928.
(3) Tarascon, J. M.; Armand, M. *Nature* **2001**, *414*, 359.
(4) Nakai, I.; Takahashi, K.; Shiraishi, Y.; Nakagome, T.; Izumi, F.; Nishikawa, F.; Konishi, T. *J. Power Sources* **1997**, *68*, 536.
(5) Padhi, A. K.; Nanjundaswamy, K. S.; Goodenough, J. B. *J. Electrochem. Soc.* **1997**, *144*, 1188.
(6) Alcantara, R.; Lavela, P.; Tirado, J. L.; Stoyanova, R.; Zhecheva, E. *J. Solid State Chem.* **1997**, *134*, 265.
(7) Denis, S.; Baudrin, E.; Touboul, M.; Tarascon, J. M. *J. Electrochem. Soc.* **1997**, *144*, 4099.
(8) (a) Suga, T.; Ohshiro, H.; Sugita, S.; Oyaizu, K.; Nishide, H. *Adv. Mater.* **2009**, *21*, 1627. (b) Oyaizu, K.; Nishide, H. *Adv. Mater.* **2009**, *21*, 2339. (c) Suga, T.; Sugita, S.; Ohshiro, H.; Oyaizu, K.; Nishide, H. *Adv. Mater.* **2011**, *23*, 751.
(9) Suga, T.; Konishi, H.; Nishide, H. *Chem. Commun.* **2007**, 1730.
(10) Jachoschka, T.; Hager, M. D.; Schubert, U. S. *Adv. Mater.* **2012**, *24*, 6397.
(11) (a) Yoshikawa, H.; Kazama, C.; Awaga, K.; Satoh, M.; Wada, J. *Chem. Commun.* **2007**, 3169. (b) Yoshikawa, H.; Hamanaka, S.; Miyoshi, Y.; Kondo, Y.; Shigematsu, S.; Akutagawa, N.; Sato, M.; Yokoyama, T.; Awaga, K. *Inorg. Chem.* **2009**, *48*, 9057.
(12) (a) Kawasaki, N.; Wang, H.; Nakanishi, R.; Hamanaka, S.; Kitaura, R.; Shinohara, H.; Yokoyama, T.; Yoshikawa, H.; Awaga, K. *Angew. Chem., Int. Ed.* **2011**, *50*, 3471. (b) Wang, H.; Hamanaka, S.; Nishimoto, Y.; Irle, S.; Yokoyama, T.; Yoshikawa, H.; Awaga, K. *J. Am. Chem. Soc.* **2012**, *134*, 4918.
(13) (a) Zhou, H.; Long, J. R.; Yaghi, O. M. *Chem. Rev.* **2012**, *112*, 673. (b) Murray, L. J.; Dincă, M.; Long, J. R. *Chem. Soc. Rev.* **2009**, *38*, 1294. (c) Mason, J. A.; Veenstra, M.; Long, J. R. *Chem. Sci.* **2014**, *5*, 32.
(14) (a) Li, J.; Sculley, J.; Zhou, H. *Chem. Rev.* **2012**, *112*, 869. (b) Kosaka, W.; Yamagishi, K.; Hori, A.; Sato, H.; Matsuda, R.; Kitagawa, S.; Takata, M.; Miyasaka, H. *J. Am. Chem. Soc.* **2013**, *135*, 18469.
(15) Inokuma, Y.; Yoshioka, S.; Ariyoshi, J.; Arai, T.; Hitora, Y.; Takada, K.; Matsunaga, S.; Rissanen, K.; Fujita, M. *Nature* **2013**, *495*, 461.
(16) Cho, S.; Ma, B.; Nguyen, S. T.; Hupp, J. T.; Albrecht-Schmitt, T. E. *Chem. Commun.* **2006**, 2563.
(17) (a) Sheberla, D.; Sun, L.; Blood-Forsythe, M. A.; Er, S.; Wade, C. R.; Brozek, C. K.; Aspuru-Guzik, A.; Dincă, M. *J. Am. Chem. Soc.* **2014**, *136*, 8859. (b) Wade, C. R.; Li, M.; Dincă, M. *Angew. Chem., Int. Ed.* **2013**, *52*, 13377. (c) Alec Talin, A.; Centrone, A.; Ford, A. C.; Foster, M. E.; Stavila, V.; Haney, P.; Adam Kinney, R.; Szalai, V.; El Gabaly, F.; Yoon, H. P.; Léonard, F.; Allendorf, M. D. *Science* **2014**, *343*, 66.
(18) (a) Férey, G.; Millange, F.; Morcrette, M.; Serre, C.; Doublet, M. L.; Grenèche, J. M.; Tarascon, J. M. *Angew. Chem., Int. Ed.* **2007**, *46*, 3259. (b) Fateeva, A.; Horcajada, P.; Devic, T.; Serre, C.; Marrot, J.; Grenèche, J. M.; Tarascon, J. M.; Maurin, G.; Férey, G. *Eur. J. Inorg. Chem.* **2010**, 3789.
(19) (a) Song, Z.; Zhan, H.; Zhou, Y. *Chem. Commun.* **2009**, 448. (b) Xu, W.; Read, A.; Koech, P. K.; Hu, D.; Wang, C.; Xiao, J.; Padmaperuma, A. B.; Graff, G. L.; Liu, J.; Zhang, J. *J. Mater. Chem.* **2012**, *22*, 4032.